Published in final edited form as:
Invest Ophthalmol Vis Sci. 2007 May ; 48(5): 1959–1967.

Bestrophin Gene Mutations Cause Canine Multifocal Retinopathy: A Novel Animal Model for Best Disease

Karina E. Guziewicz[1], **Barbara Zangerl**[1], **Sarah J. Lindauer**[1], **Robert F. Mullins**[2], **Lynne S. Sandmeyer**[3], **Bruce H. Grahn**[3], **Edwin M. Stone**[2,4], **Gregory M. Acland**[5], and **Gustavo D. Aguirre**[1]

1*From the Department of Clinical Studies, School of Veterinary Medicine, University of Pennsylvania, Philadelphia, Pennsylvania*

2*From the Department of Ophthalmology and Visual Sciences, University of Iowa Carver College of Medicine, Iowa City, Iowa*

3*From the Department of Small Animal Clinical Sciences, University of Saskatchewan, Saskatoon, Saskatchewan, Canada*

4*Howard Hughes Medical Institute, Iowa City, Iowa*

5*J.A. Baker Institute for Animal Health, Cornell University, Ithaca, New York.*

Abstract

Purpose—Canine multifocal retinopathy (*cmr*) is an autosomal recessive disorder of multiple dog breeds. The disease shares a number of clinical and pathologic similarities with Best macular dystrophy (BMD), and *cmr* is proposed as a new large animal model for Best disease.

Methods—*cmr* was characterized by ophthalmoscopy and histopathology and compared with BMD-affected patients. *BEST1* (alias *VMD2*), the bestrophin gene causally associated with BMD, was evaluated in the dog. Canine ortholog cDNA sequence was cloned and verified using RPE/choroid 5′- and 3′-RACE. Expression of the canine gene transcripts and protein was analyzed by Northern and Western blotting and immunocytochemistry. All exons and the flanking splice junctions were screened by direct sequencing.

Results—The clinical phenotype and pathology of *cmr* closely resemble lesions of BMD. Canine *VMD2* spans 13.7 kb of genomic DNA on CFA18 and shows a high level of conservation among eukaryotes. The transcript is predominantly expressed in RPE/choroid and encodes bestrophin, a 580-amino acid protein of 66 kDa. Immunocytochemistry of normal canine retina demonstrated specific localization of protein to the RPE basolateral plasma membranes. Two disease-specific sequence alterations were identified in the canine *VMD2* gene: a C_{73} T stop mutation in *cmr1* and a G_{482}A missense mutation in *cmr2*.

Conclusions—The authors propose these two spontaneous mutations in the canine *VMD2* gene, which cause *cmr*, as the first naturally occurring animal model of BMD. Further development of the

---

Corresponding author: Gustavo D. Aguirre, School of Veterinary Medicine, University of Pennsylvania, 3900 Delancey Street, Philadelphia, PA 19104; gda@vet.upenn.edu.

Supported by the Foundation Fighting Blindness; National Eye Institute/National Institutes of Health Grants EY06855, EY13132, and RO3 EY014563; Vision Research Grant P30 EY-001583; The Van Sloun Fund for Canine Genetic Research; Companion Animal Health Fund, Western College of Veterinary Medicine; and Howard Hughes Medical Institute.

Disclosure: **K.E. Guziewicz**, None; **B. Zangerl**, None; **S.J. Lindauer**, None; **R.F. Mullins**, None; **L.S. Sandmeyer**, None; **B.H. Grahn**, None; **E.M. Stone**, None; **G.M. Acland**, OptiGen LLC (I, P); **G.D. Aguirre**, OptiGen LLC (I, P)

The publication costs of this article were defrayed in part by page charge payment. This article must therefore be marked "*advertisement*" in accordance with 18 U.S.C. $1734 solely to indicate this fact.

cmr models will permit elucidation of the complex molecular mechanism of these retinopathies and the development of potential therapies.

Our population is increasingly affected by vision problems that reduce or eliminate one of the most critical human senses. Most genetically caused disorders are contributed by gene defects specifically targeting retinal structures or the neighboring retinal pigment epithelium (RPE). A current summary of human hereditary retinal disorders lists 185 mapped genetic loci; genes and causative mutations have been identified for only about two thirds of them (RetNet: http://www.sph.uth.tmc.edu/Retnet/). The investigation of hereditary disorders in humans is often limited by restriction in respective resources or number of persons segregating identical underlying mutations. This is particularly difficult when the disease phenotype develops early in life and diagnosis or potential therapy involves infants or children.

Since the late 1980s, significant progress has been made in understanding diverse aspects of the structure, function, and metabolism of the retina and RPE through numerous studies on the genetic basis and molecular mechanisms of retinal degenerative disorders in animals.[1-4] Retinal degenerations that occur naturally or are induced in laboratory species represent a large repertoire of different pathologic manifestations that are important for understanding the basis of human diseases. Similarities in phenotype between human and dog caused by underlying mutations in orthologous genes make this natural model an especially valuable one for studies of human retinopathies (for a review, see Aguirre and Acland[5]). The spectrum of inherited retinal disorders in dogs involves many breeds, and clinical features range from visual impairment to partial or total blindness, many of which have well-characterized genetic causes.[3-6]

Best macular dystrophy (BMD) is an autosomal dominant retinal disease caused by mutations in the bestrophin gene.[7,8] BMD typically presents in childhood with a striking appearance of a single, vitelliform lesion of the macula that is yolklike and is yellow to orange. However, phenotypic heterogeneity occurs, and multifocal vitelliform, atrophic lesions or chorioretinal scars have been described[8-11] (Boon C, personal communication, May 3, 2006). The disease is slowly progressive and can result in atrophy of the RPE and/or photoreceptor degeneration and often results in subretinal fibrosis, severely impairing central vision. To date, no treatment is known for Best disease.

Even though the dog lacks a foveomacular region, the ophthalmoscopic appearance of individual lesions observed in a disease termed canine multifocal retinopathy (*cmr*) closely resembles that of the vitelliform lesion of BMD. This inherited retinal abnormality has been recognized in several dog breeds, particularly Great Pyrenees (GP), Coton de Tulear (CdT), English Mastiff (EM), and Bullmastiff (Bm)[12,13] (Aguirre GD, unpublished observations). Pedigree analysis and prospective matings in the GP indicate autosomal recessive inheritance. The diseases in different breeds are broadly similar and have only minor variations. Initially, multifocal areas of retinal elevation in older dogs progress to multifocal areas of outer retinal atrophy. Concomitant RPE abnormalities have been identified on histopathologic examination.[14]

Based on the similarities between BMD and *cmr*, we undertook phenotype-directed candidate gene analysis and selected for evaluation human *BEST1* (*VMD2*), the bestrophin gene that is causally associated with BMD. We identified two distinct mutations in *VMD2* responsible for *cmr*. Based on pathologic and clinical findings, we propose *cmr* in dogs as a relevant model for Best disease in humans. In-depth characterization of the disorder will provide insight into the molecular mechanisms and potential treatments of the disease in dogs and humans.

Materials and Methods

Subjects, Samples, and Assessment

Human Patients—Patients were examined and photographed as part of their standard care. All participants in this study gave written informed consent, and institutional review board approval was obtained from The University of Iowa Human Subjects Committee in compliance with the Declaration of Helsinki. Genotyping of patients with Best disease was performed as described previously.[15]

Great Pyrenees—For the initial study, the University of Saskatchewan (Saskatoon, Canada) provided DNA and tissue samples of Great Pyrenees dogs with *cmr1*, together with previously reported pedigree and phenotype information.[12] Additional analysis was based on blood samples collected from dogs in Pennsylvania, Virginia, and Michigan.

Coton de Tulear—Phenotype ascertainment was made by one of the authors (GDA) on closely related dogs from a pedigree segregating *cmr2*; blood samples and pedigree information were provided by the breeder. In addition, DNA samples from dogs with predetermined disease status were submitted by the University of Saskatchewan.

English Mastiff, Bullmastiff, and Control Animals—Blood samples of English Mastiff and Bullmastiff dogs were obtained from a breeding colony maintained at the Retinal Disease Studies Facility (RDSF; Kennett Square, PA). DNA samples of a control dog panel, consisting of 50 unrelated animals from 12 different breeds (Irish Setter, Briard, Sloughi, Samoyed, Siberian Husky, Swedish Vallhund, Labrador Retriever, Golden Retriever, Miniature Schnauzer, German Short-haired Pointer, Newfoundland, and Mastiff) were provided (OptiGen LLC, Ithaca, NY; http://www.optigen.com/). All procedures complied strictly with the ARVO Statement for the Use of Animals in Ophthalmic and Vision Research and received Institutional Animal Care and Use Committee (IACUC) approval.

Genomic DNA was isolated from anticoagulant-preserved blood samples according to the manufacturer's instructions (QIAamp DNA Blood Mini Kit; Qiagen Inc., Valencia, CA). To ascertain genotypes of paraffin-embedded archival samples, the DNA was extracted by dissolving the paraffin sections in solution (6 μm; Cell Lysis Solution; Gentra Systems, Minneapolis, MN) at 52°C for 48 hours and was purified using the QIAquick Gel Extraction Kit (Qiagen Inc.). Phenotype ascertainment was based on clinical ophthalmic examination of dogs after pupillary dilatation with 1% tropicamide, using a binocular indirect ophthalmoscope with or without additional direct ophthalmoscopy and biomicroscopy with a hand-held slit lamp (SL-14; Kowa, Torrance, CA). Fundus photographs were taken with a fundus camera (RC-2; Kowa) and film (Kodachrome 25; Eastman Kodak, Rochester, NY) either directly or through a panretinal clear indirect ophthalmoscopy lens (2.2; Volk, Mentor, OH).

Retinal Pathology of *cmr1*

We obtained paraffin blocks of eyes from clinically phenotyped GP dogs (1 healthy, 1 year old; 2 affected, 4 and 10 years old). Tissues from these archival samples had been fixed in Bouin solution, rinsed, and stored in 70% ethanol before paraffin sectioning and routine embedding.[12] Tissue sections were stained with hematoxylin and eosin (H&E) and periodic acid Schiff (PAS) or were coverslipped unstained with xylene and examined with a microscope (Axioplan; Carl Zeiss Meditech, Oberkochen, Germany) using transmitted light with or without differential interference optics (DIC) or epifluorescence (FITC excitation filter, 450 – 490 nm; Carl Zeiss). Images were digitally captured (Spot 3.3 camera; Diagnostic Instruments, Inc., Sterling Heights, MI) and imported into a graphics program (Photoshop; Adobe, Mountain View, CA) for display.

Retinal Pathology of Best Disease

The eye of an 86-year-old donor with a heterozygous T6R mutation in *VMD2* was obtained approximately 8.5 hours after death, and a wedge of the inferotemporal retina/RPE/choroid was fixed in 4% formaldehyde/PBS (prepared from paraformaldehyde). The tissue was infiltrated in sucrose, embedded in optimal cutting temperature (OCT), and sectioned at 7 μm. Sections were examined under a microscope (BX-41; Olympus, Tokyo, Japan) using transmitted light or epifluorescence.

Cloning and Characterization of Canine *VMD2*

Gene-specific primers were designed on the predicted canine *VMD2* sequence (http://genome.ucsc.edu/) using the Primer3 software (http://frodo.wi.mit.edu/primer3/primer3_code.html; Supplementary Table S1, online at http://www.iovs.org/cgi/content/full/48/5/1959/ DC1). The complete cDNA sequence of canine *VMD2* was verified by constructing RPE/choroid 5′- and 3′-RACE libraries (BD Smart Race cDNA Amplification Kit; Clontech, Mountain View, CA) according to the manufacturer's protocol and then were cloned into pCR 2.1-TOPO vector (Invitrogen, Carlsbad, CA) using a cloning kit according to the manufacturer's instructions (TOPO TA Cloning kit; Invitrogen).

Promoter regions of *VMD2* were screened through the CONSITE database (http://mordor.cgb.ki.se/cgi-bin/CONSITE/consite) for dog, human, and mouse (http://genome.ucsc.edu/).

Gene alignments were assembled from experimental data or hypothetical loci for human (*Homo sapiens*, NM_004183; NP_004174), chimpanzee (*Pan troglodytes*, XM_522029; XP_5220291), rhesus monkey (*Macaca mulatta*, ENSG00000167995), crab-eating macaque (*Macaca fascicularis*, AY357925.1; AAQ56049), cow (*Bos taurus*, scaffold130366.2; XP_585778), pig (*Sus scrofa*, AY064707, BI343182; AAL40882), mouse (*Mus musculus*, NM_011913; NP_036043), rat (*Rattus norvegicus*, XM_574621; NP_001011940), chicken (*Gallus gallu*s, XM_421055; XP_421055), opossum (*Monodelphis domestica*, scaffold14923.4), zebrafish (*Danio rerio*, ENSDART00000007569.2; XP_689098), xenopus (*Xenopus tropicalis*, CR760914; NP_988974), *Drosophila* (*Drosophila melanogaster*, NM_144346; NP_652603), and *Caenorhabditis elegans* (*C. elegans*, NM_061231; NP_493632.1). Proposed reading frames for the chicken and opossum were shortened at the 5′-end to start at the same position suggested for all other species. Hypothetical sequences posted for the chimpanzee and cow were modified at the 3′-end to splice into exon 11 at the same site as the orthologous human sequence; in the same manner, the predicted dog open-reading frame was corrected, matching the C-terminal protein sequence with that found in other nonrodent mammals. Finally, the published pig sequence did not have exons 1 to 3 or part of exon 4. The complete gene was reconstructed through an independent EST (BI343182) representing the beginning of the pig *VMD2* (however, the complete pig *VMD2* sequence is missing 25 bp in exon 4 that have not yet been sequenced).

Multiple nucleotide and protein sequence alignments were derived using CLUSTAL W, with a gap penalty of 10 and a gap extension penalty of 0.2. The nucleotide distance was based on a bootstrapped (n = 1000) F84 model.[16] Protein distances were calculated using a bootstrapped (n = 1000) Jones-Taylor-Thornton model, and the protein weight matrix was Blossom 30. An overall phylogenetic tree was inferred from the multiple sequence alignment using PHYLIP (version 3.5c) based on a neighbor-joining algorithm.[16]

VMD2 Expression Study

RNA Extraction and Reverse Transcription—Standard Trizol extraction was used to isolate total RNA from eight different tissues of a healthy 16-week-old male beagle. First-

strand cDNA was generated from 5 μg total RNA (SuperScript II reverse transcriptase, 50 U; Invitrogen, Grand Island, NY), anchored random hexamers primers (50 ng/μL), and RNase inhibitor (RNaseOUT, 40 U; Invitrogen). cDNA synthesis was performed at 42°C for 50 minutes, followed by 20-minute RNase H treatment (2 U; Invitrogen). The quality of cDNA synthesis was assessed by PCR amplification of glyceraldehyde-3-phosphate dehydrogenase (*GAPDH*) as a housekeeping gene using a combination of forward (5′-TGGTGCTGAGTATGTAGTGG-3′) and reverse (5′-TGGGTGTCACTGTTGAAGTC-3′) primers. The 329-bp fragment of *VMD2*, spanning exons 3 to 5, was amplified by RT-3F and RT-3R gene-specific primers (Supplementary Table S1).

Northern Blot Analysis—Northern blot analysis was carried out as described previously[17] with 10 μg total RNA of each desired tissue (RPE/choroid, retina, and brain). A 329-bp fragment of canine *VMD2*, amplified with primers RT-3F and RT-3R (Supplementary Table S1), was labeled with α-dCTP-P^{32} using the RadPrime DNA labeling System (Invitrogen) and used as a probe for Northern blot analysis.

Western Blot Analysis—Total protein was extracted from the RPE/choroid of a 16-week-old healthy dog in 1 mL 1× Laemmli buffer, and 10 μg extract was run on 10% polyacrylamide gel electrophoresis and transferred to a transfer membrane (Immobilon; Millipore, Billerica, MA). A primary bestrophin mouse anti– human monoclonal antibody E6–6[18] was applied at a 1:400 dilution and was visualized with a rabbit anti–mouse IgG HRP secondary antibody (Zymed, Carlsbad, CA) with the use of detection reagent (ECL Western Blotting Detection Reagents Kit; Amersham, Piscataway, NJ) after 1 second of exposure to x-ray film.

Immunocytochemistry—Normal retinas from dogs and other species (*Felis catus, M. fascicularis, Equus caballus*, and *R. norvegicus*) were fixed in 4% paraformaldehyde, embedded in OCT medium, and cut at 10 μm as previously described.[19] Tissue sections were washed with 1× PBS/0.25% Triton X-100 and, after treatment with blocking buffer (10% normal goat serum [NGS], 1× PBS/0.25% Triton X-100, 0.05% sodium azide), were incubated overnight at 4°C with bestrophin mouse anti– human monoclonal antibody E6–6 or with rabbit anti– human polyclonal antibody Pab-125.[18] As a secondary antibody, goat anti–mouse or goat anti–rabbit antibody was used (1:5000; Zymed, San Francisco, CA). Sections were examined under a microscope (Axioplan; Carl Zeiss) using epifluorescence, and images were captured and processed as described.

Mutation Screening of Canine *VMD2*

Coding exons and flanking splice junctions of canine *VMD2* were analyzed by PCR amplification and direct sequencing. All sequencing products were run (ABI 3730 sequencer; Applied Biosystems, Foster City, CA) at the DNA Sequencing Facility of the University of Pennsylvania in Philadelphia and were evaluated with the use of a software package (Sequencher 4.2.2).

$C_{73}T$ (*cmr1*) and $G_{482}A$ (*cmr2*) mutations were confirmed by sequencing of both strands after PCR using primer pairs Ex2-1F and Ex2R, which generated the 212-bp product for the $C_{73}T$ substitution, or Ex5F and Ex5R, which amplified the 387-bp band for the $G_{482}A$ alteration (Supplementary Table S1). Further assessment of the $C_{73}T$ mutation for *cmr1* was made on the same 212-bp PCR fragment by restriction digestion with *Hph*I (New England Biolabs, Ipswich, MA). The digestion gave bands of 144 and 68 bp (mutant) or 212, 144, and 68 bp (carrier); the 212-bp PCR product of normal control remained undigested. The absence of the $G_{482}A$ mutation in control dog panel was verified by the amplification refractory mutation system (ARMS), with Ex5F as an anchor primer and ARMS1 as a discriminatory primer for

the wild-type allele or ARMS2 as a discriminatory primer for the mutant allele (Supplementary Table S1).

Results

Canine Multifocal Retinopathy: Ophthalmoscopic and Pathologic Findings

Salient fundus changes are usually present in animals affected with *cmr* before 4 months of age and are characterized by multifocal areas of retinal elevation that contain subretinal accumulation of serous to pink-tan fluid (compare Fig. 1A with 1B_1-E). Focal elevations are most clearly visible by ophthalmoscopy in the superior quadrants (tapetal zone), and some lesions are partially delimited by an incomplete ring of retinal edema (Figs. 1D, 1E, arrows). In the more densely pigmented inferior quadrants (nontapetal zone), the lesions are white, fewer in number, and often located near or adjacent to the inferior retinal vessels. The difference in appearance and shape of the lesions, depending on the location, is likely the result of the lack of RPE pigmentation of the tapetal zone and of differences in the vascular anatomy of the choroid, particularly the choriocapillaris, between the two regions.[20] Retinal elevations can remain static for several years, whereas multifocal outer retinal atrophy is often seen in older animals.

We obtained archival paraffin blocks of eyes that were fixed in Bouin solution from 3 GP dogs, 1 nonaffected and 2 affected. *VMD2* genotype was confirmed by mutation analysis using genomic DNA isolated from the tissue sections and demonstrated that the nonaffected dog was homozygous normal and that both affected dogs were homozygous for the stop mutation in *VMD2*, now termed *cmr1* to differentiate it from a second missense mutation in *VMD2* called *cmr2*. The eyes had been sectioned in the dorsoventral plane in the pupil– optic nerve axis, with no special attempt to orient the tissue block in relation to the clinically evident fundus lesions. Additional eyes or tissue blocks from younger *cmr1*-affected dogs, or any dogs with *cmr2*, were unavailable for study.

Compared with the normal adult control retina, the retina of the young affected dog showed that the nonpigmented RPE cells of the tapetal region were hypertrophic and had a slightly "scalloped" apical border (Fig. 2; compare normal [Fig. 2A] with mutant [Figs. 2B, 2B_1–B_3]). The cytoplasm had a homogeneous-to-granular, tan-to-light brown pigment. Larger brown inclusions were occasionally observed. Peripheral RPE superi-orly was densely pigmented, and the cytoplasmic content was difficult to evaluate. Similarly, the central half of the inferior RPE showed the same findings, though these were less dramatic because of the dense melanin pigment content of the cells. Epifluorescence microscopy of unstained sections showed the accumulation of fine-granular autofluorescent granules in the hypertrophied cells. Although fixation-associated autofluorescence of all ocular tissues—particularly collagenous fibers—was observed in healthy control and affected dogs, control RPE cells were not hypertrophied and showed no accumulation of autofluorescent cytoplasmic granules (Fig. 2; compare normal [Figs. 2A_1,2A_2] with mutant [Figs. 2B_4,2B_5]).

The eye of the older affected dog showed extensive disease affecting the RPE and neural retina (Fig. 3). In the periphery, retinal atrophy was advanced to nearly full thickness with foci where the RPE was lost, and the disorganized atrophic retina was fused to Bruch membrane (BM). More centrally, some RPE cells were hypertrophied and had large, granular PAS+ inclusions, some which appeared to form clumps. Even in cells not hypertrophied, granular PAS+ material accumulated in RPE cells. Centrally, there were areas of focal to extensive retina–BM fusions, and the RPE was absent. Interspersed between these areas of RPE and retinal atrophy, we found one region near the superior optic nerve head in which normal retinal structure was present. Two other small foci in the superior quadrant showed partial preservation of the outer retinal layers; in these areas, numbers of photoreceptor inner and outer segments were decreased and

reduced in length, and the outer nuclear layer was 2 to 3 nuclei wide. As in most other areas in which RPE was present, the cells had tan-brown cytoplasmic granular material that was PAS +, and BM was thickened and intensely PAS+. Epifluorescence microscopy showed that the granular material accumulating in all the RPE cells was autofluorescent.

Best Disease: Multifocal Fundus Changes and Histopathologic Findings

Although typical lesions in Best disease are subfoveal and smaller than two disk diameters, multifocal lesions also are observed. Figure 1 illustrates 30° (Fig. 1F) and 60° (Fig. 1G) fundus photographs of the right eyes of patients with multifocal Best disease. One 41-year-old patient had a heterozygous A243T mutation in *VMD2* (Fig. 1F), and another patient carried a Y227N variation (Fig. 1G). Both patients exhibited yellow deposits (Figs. 1F, 1G; arrowheads) well outside the fovea that were funduscopically similar to the multifocal lesions observed in the canine model.

In addition, the histopathologic abnormalities present in late-stage Best disease were similar to those of *cmr1*. Figure 3 illustrates bright-field (Fig. $3E_1$, Fig. $3F_1$) and epifluorescence (Fig. $3E_2$, Fig. $3F_2$) images of the retina of an 86-year-old patient with a heterozygous T6R mutation in *VMD2*. The fovea of this eye had a large disciform scar (not shown), and the lesions illustrated are outside the fovea. Clusters of pigmented cells, either RPE or melanophages, are present, and extensive intracytoplasmic lipofuscin accumulation results in bright, granular autofluorescence. Areas of photoreceptor loss are associated with regions of RPE dropout, but BM is intact. Additional histopathologic features of this eye are part of a separate report.[21]

Comparative Analysis of the *VMD2* Gene and Mutation Identification

Structure and Sequence—BMD previously was mapped to the long arm of HSA 11q13, and *VMD2* and disease-causing mutations were identified by positional cloning combined with candidate gene analysis.[22,23] Human *VMD2* spans a genomic region of 14.1 kb with a 1755-bp open-reading frame divided into 11 exons. The canine ortholog of *VMD2* is located on chromosome 18 (57,498,216 –57,511,980) and is flanked by *RAB3IL1* and *FTH1* (http://genome.ucsc.edu/; Ref. 24). To evaluate the association of the *VMD2* gene with *cmr*, the complete cDNA sequence in the dog was cloned and verified by 5′- and 3′-RACE. The canine gene has a 1740-bp open-reading frame and consists of 11 exons, differing in the 3′ end from the prediction deduced from the genome draft, with its translation initiation codon in exon 2, as observed in the human ortholog (GenBank accession no. EF110978).

Comparative nucleotide sequence analysis demonstrated that canine *VMD2* is highly conserved across 14 eukaryotes analyzed (Fig. 4), sharing 41% to 99% sequence identity between individual pairs of species (data not shown), 86% with the human gene, and 77% with the murine ortholog. The closest relationship to humans based on sequence identity is observed with apes (99%) and macaques (97%), and then with dogs (86%); *C. elegans* proves to be the most distant relative (44%). Comparative analysis of the translated protein sequence demonstrated that canine bestrophin differs by approximately 20% in amino acid sequence from the human ortholog. The N-terminal end of the protein is highly conserved across 14 eukaryotes (divergence, 0%– 42%), including evolutionarily distant organisms such as *D. melanogaster* and *C. elegans*, whereas the C-terminal part of the polypeptide is more divergent.

Promoter Region Motifs—Comparisons of approximately 1.2-kb sequence from the 5′-untranslated region of human, mouse, and dog *VMD2* revealed numerous consensus sequences characterizing the gene-promoter region. Within the analyzed sequences, E-box 2-, Crx/Otx1-, and Crx/Otx2-binding sites are well conserved in the three species. Similar to the human and murine genes, the consensus TATA and CAAT boxes are not present at typical positions in the dog sequence.[25] In addition, the 5-kb genomic sequence upstream of the *VMD2* start codon

was compared for the human, mouse, and dog and resulted in the identification of new, potentially regulatory, regions. Among several blocks of consensus transcription factor–binding sites conserved between species pairs, two were completely conserved in all three sequences. The first one (AGTCAAGTGA) is located 180 bp upstream from the dog ATG sequence and has multiple potential factors binding to the motif (Max, ARNT, Snail, USF, n-MYC). The second one (CACCTGCTGCAG) recognized a Myf-binding site and is positioned 26 bp in front of the start codon. Promoter region analysis could not be performed with more distant species because of problems in the alignment of ortholog loci (*G. gallus* and *M. domestica*) or because of lack of factors shared between more than two species. Interestingly, the comparison of the canine 5′-untranslated region to the upstream region in *D. melanogaster* identified another ARNT/USF/n-MYC complex 1078 bp upstream from the initiation ATG in the canine sequence that showed a high degree of sequence conservation between the two species. Functional analysis to determine the importance of these structures is under way.

Expression of VMD2 Transcripts and Protein—Encoded by the *VMD2* gene is a 585-amino acid bestrophin transmembrane protein belonging to the family of anion channel proteins.[26] Comparable to findings in humans, the 2.1-kb canine *VMD2* mRNA is found to be primarily expressed in the RPE/ choroid, though lower levels of expression also have been identified by RT-PCR in retina and brain. On Northern blot analysis, a distinct, robust signal is present only in RPE/choroid and not in retina or brain (Figs. 5A, 5B). The canine bestrophin protein is only five amino acids shorter than the human bestrophin protein and has a calculated molecular weight of 66 kDa. Western blot analysis using mouse anti– human monoclonal antibody E6–6[18] confirmed that the antibody recognized a single protein band of the appropriate size in normal canine RPE/choroid tissue (Fig. 6C). Retinal or RPE/choroid tissues from *cmr1*-or *cmr2*-affected dogs were unavailable for expression analyses.

Immunocytochemistry with anti– human monoclonal antibody E6–6 in normal canine retina fixed in 4% paraformalde-hyde and embedded in OCT demonstrated specific localization of bestrophin to the basolateral plasma membranes of the RPE cells (Figs. $6A_1$, $6A_2$). Similar results were obtained with rabbit polyclonal antibody Pab-125.[18] The same E6–6 antibody detected intense, specific bestrophin labeling in the RPE of *M. fascicularis* and *F. catus* (Figs. 6B, 6C) and weak labeling in *E. caballus* but not in *R. norvegicus* because of a lower level of sequence conservation (data not shown). These antibodies did not label the RPE of the paraffin embedded normal or *cmr1*-affected dogs used for histopathologic analysis of the disease, even after antigen retrieval.

Sequence Analysis and Identification of *cmr*-Associated Mutations—Direct sequencing of all coding exons and exon–intron junctions of canine *VMD2* identified a nonsense mutation associated with the disease in GP, EM, and Bm dogs (*cmr1*), and a missense mutation in a CdT pedigree (*cmr2*; Figs. 7A, 7B). In 4 *cmr1*-affected GP dogs, a homozygous single nucleotide change in exon 2 at codon 25 of the *VMD2* coding sequence ($C_{73}T$) was observed to cosegregate with the disease allele, whereas three verified obligate carriers were heterozygous. In two phenotypically normal members of a previously described GP pedigree,[12] the mutation was not present. The $C_{73}T$ transition results in replacement of the Arg_{25} residue with a stop codon and creates a new *Hph*I restriction site. The same change was found in GP-related breeds, EM and Bm dogs, with clinically and phenotypically similar disease (Ref. 27 and BH Grahn, unpublished data, 2006). In all seven *cmr2*-affected animals analyzed from the CdT breed, a homozygous guanine-to-adenine transition ($G_{482}A$) in exon 5 was detected, resulting in a $Gly_{161}Asp$ substitution. All five available obligate carriers were heterozygous for the change, but the nucleotide variation was not present in any of 29 phenotypically normal animals of the CdT pedigree.

Sequence comparison between sequences of *VMD2* obtained from CdT and GP breeds with the canine SNP database (http://www.broad.mit.edu/mammals/dog/snp/) confirmed that the described mutations, together with 11 rare, benign breed-specific DNA variants, have not previously been known (Supplementary Table S2, online at http://www.iovs.org/cgi/content/full/48/5/1959/DC1). Furthermore, *cmr1* and *cmr2* mutations were not present in 100 control chromosomes from 50 dogs of 12 breeds examined (data not shown). Positions G_{482} and C_{73} are completely conserved in all examined mammals, *Xenopus tropicalis*, and *D. melanogaster*. Moreover, G_{482} and its residue, Gly_{161}, are evolutionarily conserved at this position across all analyzed eukaryotes, including *G. gallus*, *D. rerio*, and *C. elegans*.

Discussion

The RPE is crucial for the normal development, function, and maintenance of retinal photoreceptors. Several genes preferentially expressed in the RPE, such as *RPE65*, *Mertk*, and *VMD2*, have been causatively linked to naturally occurring retinal diseases in humans and animals (Ref. 2 and present study). Mutations in one of these, *VMD2*, are the cause of BMD, a severe juvenile macular disease that shows variable expressivity in age of onset, clinical findings, progression, and even final visual outcome.[10,28] To date, more than 100 Best disease–associated variants have been identified[8]; most represent missense changes, predominantly concentrated within the N- terminus, suggesting the functional significance of this particular bestrophin domain.[23,29] An unexplained high clinical heterogeneity of Best disease results from these changes. Thus, generally four criteria are required for the diagnosis of BMD: typical fundus changes, autosomal dominant inheritance, subnormal electro-oculogram (EOG), and typical onset and natural disease course.[28] However, exceptions to one or more of these occur, a possible indication that the requirements represent recommended criteria rather than prerequisites for diagnosis.

For example, variable expressivity and incomplete penetrance is well accepted,[11,28] and approximately 5% of patients with *VMD2* mutations have normal or minimally abnormal macular findings.[30] Some mutation-positive asymptomatic patients may have delayed expression of the clinical pheno-type.[10] One salient example of incomplete penetrance was recently reported.[11] Two female siblings who were compound heterozygotes (Tyr_{29}stop/Arg_{141}His) had early-onset visual symptoms and characteristic vitelliform macular lesions. Both the parents (father, Tyr_{29}stop/+; mother, Arg_{141}His/+), and the children (Tyr_{29}stop/+) of one of the patients had unremarkable fundi and normal visual acuity. However, EOG results were abnormal in patients and parents. Based on this and other studies,[8,31] it appears that of all the criteria used to establish a diagnosis of BMD, one of the most reliable and invariant—though exceptions do occur—is subnormal EOG findings.[28,32,33]

To examine the underlying molecular mechanisms of BMD, experimentally created rodent bestrophin models have been produced that include knock-out/knock-in mice and rats with adenoviral-mediated bestrophin overexpression.[34,35] Although these models have provided critical information about bestrophin function,[26,36,37] none has been a phenotypic replica of the human disease (Marmorstein A. *IOVS* 2006;47:ARVO E-abstract 126). Therefore, establishing an animal model that closely mimics the human phenotype and pathology will be important to address experimentally the complexity of the disease.

The $R_{25}X$ mutation identified in *cmr1* is located in the critical N-terminal domain and the previously reported codon 25 mutational hot spot of *VMD2*: $R_{25}Q$[38] and $R_{25}W$.[39] In GP, EM, and Bm dogs, the $C_{73}T$ mutation causes a premature translation termination that limits the open-reading frame to 25 codons, compared with 580 codons in the wild-type mRNA. Although not yet established experimentally, we posit that this nonsense mutation results in a null-allele resulting from nonsense-mediated RNA degradation.[40]

In contrast, the missense mutation responsible for *cmr2* in CdT is a $G_{482}A$ transition that changes an evolutionarily conserved glycine residue to aspartic acid. Genotyping independent populations of related and unrelated animals confirmed the genotype–phenotype correlation for this mutation. Thus, all seven samples of *cmr2*-affected CdT dogs were homozygous mutant, whereas five clinically normal obligate carriers were heterozygous. Further analysis of 50 phenotypically normal animals of 12 different breeds did not identify any animals with aspartic acid at position 161. These data, taken together with the fact that glycine at residue 161 is fully evolutionarily conserved, support the conclusion that the G3 A transition in *VMD2* is the disease-causing mutation. We speculate that the replacement of glycine, a small hydrophobic and uncharged amino acid, with the larger, polar, and negatively charged aspartic acid is drastic enough to create a phenotype indistinguishable from the *cmr1*-affected dogs carrying the nonsense mutation. Our finding suggests that this mutation renders the affected protein nonfunctional and has an effect comparable to the proposed null-allele of *cmr1*. These hypotheses remain to be tested.

To estimate the exact influence of such an amino acid substitution, it is critical to better understand the structure and function of the bestrophin protein. Despite major efforts by multiple groups (for a review, see Hartzell et al.[29]), the folding and structural domains of bestrophin are still unclear. Several in silico attempts to localize domains and to describe functional relations for the mutated amino acids have not yielded J scores in 3D-Jury higher than 50, the minimum value for a reasonable prediction (Ripoll D, Cornell University, personal communication, November 10, 2005). Moreover, high conservation levels of nucleotide and protein sequences of *VMD2* and of particular transcription factors in the promoter region suggest a persistent importance of the gene throughout the evolutionary differentiation of eukaryotes. Once the described models are developed and characterized, it may be possible to address some of these critically important biological questions.

Based on the criteria used for establishing a diagnosis for BMD and the available clinical, pathologic, and molecular results for *cmr*, it is important to establish how the canine model compares with the disease in humans.

Typical Fundus Changes

Original findings in patients with BMD described focal vitelliform lesions limited to the macular region, but patients with multifocal disease, which in general also includes macular abnormalities, have been reported (Ref. 41 and Boon C, personal communication, May 3, 2006). These lesions, and their progression, appear similar in human and canine patients (Fig. 1). However, the canine retina, unlike the human retina, lacks a distinct foveomacular region though an area centralis is present.[42] Such anatomic constraints preclude “macular” abnormalities and favor the development of multifocal rather than focal disease. In addition, differential distribution of the lesions between the two species could be attributed to different gene expression levels in the RPE between species or to the presence of redundant canine-specific isoforms. Alternatively, because *VMD2* expression levels appear to be lowest in the human macular region, the paucity of bestrophin in the macula may predispose this region to disease.[21] If one considers the animal model as an important adjunct to develop and test potential therapies, multifocal disease is preferable for localized therapies because the untreated regions of the same eye can be used as control.

Autosomal Dominant Inheritance

Both *cmr1* and *cmr2* are autosomal recessive disorders. Ophthalmoscopic examination of obligate heterozygous animals with either disease reveals normal fundi. Because practices used in the breeding of purebred dogs intensify homozygosity at different genetic loci,[43] it is not surprising to find that most affected dogs are homozygous mutant for the different *cmr* alleles

identified in each respective breed. The variable expression and incomplete penetrance of *VMD2* mutations recognized in humans may also occur in dogs. Given that the total number of heterozygote animals examined is small, it is possible that a larger sample of genotype-ascertained heterozygotes would show clinical disease in terms of fundus changes when examined serially.

Subnormal EOG

Electro-oculography is not used routinely in the diagnosis of retinal disorders in large animal models of human retinal disease. Based on human and rodent data[28] (Marmorstein A. *IOVS* 2006;47:ARVO E-abstract 126), we would anticipate EOG abnormalities in clinically normal heterozygotes; such studies are in progress.

Typical Onset and Natural Disease Course

Unlike human patients with variable disease expressivity regarding age of onset, clinical findings, progression, and even final outcome,[10,28] canine disease in homozygous affected animals is uniform; it has a juvenile onset, before 4 months of age, and a predictable natural disease course. This can likely be attributed to a more uniform genetic background resulting from modern dog breed evolution.

With the use of criteria outlined in these subsections, the similarities between BMD and *cmr* indicate that the dog is a highly relevant model for the human disease. In addition, abnormalities described for *cmr* in this study (e.g., RPE hypertrophy, accumulation of autofluorescent lipopigments, RPE hypertrophy and loss, chorioretinal scars [see, for example, Mullins et al.[10] and Hoppe et al.[44]]), further emphasize the similarities between canine and human disease resulting from *VMD2* mutations.

Previous data and results from the present study show that although *VMD2* mRNA has been found in the RPE, retina, brain, testis and placenta, the protein has only been detected in the RPE cell layer.[37] Moreover, the biocomputation transmembrane domain prediction[29] and immunocytochemical analysis of bestrophin localization[23] provide evidence that the *VMD2* gene product is an integral part of the plasma membrane and is restricted to the basolateral regions of the RPE cells in human,[44] mouse,[36] and dog (Fig. 6). The proposed model of bestrophin topology situates the $G_{161}D$ substitution in the intracellular loop, near the third transmembrane domain, a region of unexplored structural and functional features.[29] Additional studies in elucidating the significance of this domain in the bestrophin protein, together with functional assays such as structural modeling of mutated protein and in vitro analysis on the properties of the wild-type and mutant canine bestrophin proteins, will be required to determine the exact consequences of the $G_{161}D$ transition. Together with the molecular characterization of the *cmr1* stop mutation, these studies will provide new information of the molecular mechanisms of disease resulting from *VMD2* mutations in the canine models.

In summary, our studies show a high level of identity between canine *VMD2* and its orthologs among divergent species. This implies a critical functional role for the protein in inherited retinopathies confirmed by our identification of two distinct mutations in canine *VMD2* associated with *cmr*. These studies constitute the preliminary description of a novel canine model of human inherited retinopathy. Because these are naturally occurring diseases in the canine population and, hence, are unavailable for experimental studies, the models are now under development in research colonies to take full advantage of this unique resource. Having a model that so closely resembles human retinal disease will allow us not only to study the complexity of the disease mechanism but also to explore gene-based and other experimental therapy approaches that can be developed and validated in dogs before use in human patients.

Acknowledgments

The authors thank Daniel Ripoll from Cornell University for assistance and consultation on bestrophin protein modeling; Alan Marmorstein from the University of Arizona for providing bestrophin antibodies, helpful advice, suggestions, and prepublication material; Patrik Schatz from University of Lund and Camiel Boon from Radboud University Nijmegen for providing prepublication manuscripts; Stephen Gross for phenotype ascertainment on selected CdT dogs; Carolyn Brooke for invaluable help in developing informative *cmr2* pedigrees for analysis; Diane and Judy Skorup for collecting blood samples from dogs at risk for *cmr1*; and Sue Pearce-Kelling for excellent technical assistance. Control samples were provided by OptiGen LLC (Ithaca, NY).

References

1. Akhmedov NB, Piriev NI, Chang B, et al. A deletion in a photoreceptor-specific nuclear receptor mRNA causes retinal degeneration in the rd7 mouse. Proc Natl Acad Sci USA 2000;97:5551–5556. [PubMed: 10805811]
2. D'Cruz PM, Yasumura D, Weir J, et al. Mutation of the receptor tyrosine kinase gene Mertk in the retinal dystrophic RCS rat. Hum Mol Genet 2000;9:645–651. [PubMed: 10699188]
3. Kijas JW, Cideciyan AV, Aleman TS, et al. Naturally occurring rhodopsin mutation in the dog causes retinal dysfunction and degeneration mimicking human dominant retinitis pigmentosa. Proc Natl Acad Sci USA 2002;99:6328–6333. [PubMed: 11972042]
4. Cideciyan AV, Jacobson SG, Aleman TS, et al. In vivo dynamics of retinal injury and repair in the rhodopsin mutant dog model of human retinitis pigmentosa. Proc Natl Acad Sci USA 2005;102:5233–5238. [PubMed: 15784735]
5. Aguirre, GD.; Acland, GM. Models, mutants and man: searching for unique phenotypes and genes in the dog model of inherited retinal degeneration. In: Ostrander, EA.; Giger, U.; Lindblad-Toh, K., editors. The Dog and Its Genome. Cold Spring Harbor Laboratory Press; Cold Spring Harbor, NY: 2006.
6. Zangerl B, Goldstein O, Philp AR, et al. Identical mutation in a novel retinal gene causes progressive rod-cone degeneration in dogs and retinitis pigmentosa in humans. Genomics 2006;88:551–563. [PubMed: 16938425]
7. Best F. Ueber eine hereditaere Maculaaffektion. Z Augenheilkunde 1905;13:199–212.
8. Lorenz B, Preising MN. Best's disease: overview of pathology and its causes. Ophthalmologe 2005;102:111–115. [PubMed: 15657691]
9. Maruko I, Iida T, Spaide RF, Kishi S. Indocyanine green angiography abnormality of the periphery in vitelliform macular dystrophy. Am J Ophthalmol 2006;141:976–978. [PubMed: 16678528]
10. Mullins RF, Oh KT, Heffron E, et al. Late development of vitelliform lesions and flecks in a patient with best disease: clinicopathologic correlation. Arch Ophthalmol 2005;123:1588–1594. [PubMed: 16286623]
11. Schatz P, Klar J, Andreasson S, et al. Variant phenotype of Best vitelliform macular dystrophy associated with compound heterozygous mutations in VMD2. Ophthalmic Genet 2006;27:51–56. [PubMed: 16754206]
12. Grahn BH, Philibert H, Cullen CL, et al. Multifocal retinopathy of Great Pyrenees dogs. Vet Ophthalmol 1998;1:211–221. [PubMed: 11397233]
13. Grahn, BH.; Sandmeyer, LS.; Breaux, CB. Retinopathy of Coton de Tulear dogs; Presented at: American College of Veterinary Ophthalmologists 36th Annual Conference; Nashville, TN. November 2–4, 2005;
14. Grahn BH, Cullen CL. Retinopathy of Great Pyrenees dogs: fluorescein angiography, light microscopy and transmitting and scanning electron microscopy. Vet Ophthalmol 2001;4:191–199. [PubMed: 11722783]
15. Lotery AJ, Munier FL, Fishman GA, et al. Allelic variation in the VMD2 gene in Best disease and age-related macular degeneration. Invest Ophthalmol Vis Sci 2000;41:1291–1296. [PubMed: 10798642]
16. PHYLIP (Phylogeny Inference Package) (computer program). Version 3.5c. Department of Genetics, University of Washington; Seattle, WA: 1993. CladisticsDistributed by the author (Felsenstein J)

17. Goldstein O, Zangerl B, Pearce-Kelling S, et al. Linkage disequilibrium mapping in domestic dog breeds narrows the progressive rod-cone degeneration interval and identifies ancestral disease-transmitting chromosome. Genomics 2006;88:541–550. [PubMed: 16859891]
18. Marmorstein AD, Marmorstein LY, Rayborn M, et al. Bestrophin, the product of the Best vitelliform macular dystrophy gene (VMD2), localizes to the basolateral plasma membrane of the retinal pigment epithelium. Proc Natl Acad Sci USA 2000;97:12758–12763. [PubMed: 11050159]
19. Beltran WA, Rohrer H, Aguirre GD. Immunolocalization of ciliary neurotrophic factor receptor alpha (CNTFRα) in mammalian photoreceptor cells. Mol Vis 2005;11:232–244. [PubMed: 15827545]
20. Aguirre, GD.; Ray, J.; Stramm, LE. Diseases of the retinal pigment epithelium–photoreceptor complex in non-rodent animal models. In: Marmor, MF.; Wolfensberger, TJ., editors. RetinalPigmentEpithelium—Current Aspects of Function and Disease. Oxford University Press; New York: 1998.
21. Mullins RF, Kuehn MH, Faidley EA, Syed NA, Stone EM. Periphery to macula gradient of bestrophin expression in human eyes and its implication for Best Disease. Invest Ophthalmol Vis Sci. In press
22. Stone EM, Nichols BE, Streb LM, et al. Genetic linkage of vitelliform macular degeneration (Best's disease) to chromosome 11q13. Nat Genet 1992;1:246–250. [PubMed: 1302019]
23. Petrukhin K, Koisti MJ, Bakall B, et al. Identification of the gene responsible for Best macular dystrophy. Nat Genet 1998;19:241–247. [PubMed: 9662395]
24. Lindblad-Toh K, Wade CM, Mikkelsen TS, et al. Genome sequence, comparative analysis and haplotype structure of the domestic dog (comment). Nature 2005;438:803. [PubMed: 16341006]
25. Esumi N, Oshima Y, Li Y, et al. Analysis of the *VMD2* promoter and implication of E-box binding factors in its regulation. J Biol Chem 2004;279:19064–19073. [PubMed: 14982938]
26. Sun H, Tsunenari T, Yau KW, Nathans J. The vitelliform macular dystrophy protein defines a new family of chloride channels. Proc Natl Acad Sci USA 2002;99:4008–4013. [PubMed: 11904445]
27. Grahn BH, Sandmeyer LS. Multifocal retinopathy of Great Pyrenees dogs. Can Vet J 2006;47:491–492. [PubMed: 16734379]
28. Wabbels B, Preising MN, Kretschmann U, Demmler A, Lorenz B. Genotype-phenotype correlation and longitudinal course in ten families with Best vitelliform macular dystrophy. Graefes Arch Clin Exp Ophthalmol 2006;244:1453–1466. [PubMed: 16612637]
29. Hartzell C, Qu Z, Putzier I, et al. Looking chloride channels straight in the eye: bestrophins, lipofuscinosis, and retinal degeneration. Physiology (Bethesda) 2005;20:292–302. [PubMed: 16174869]
30. Blodi CF, Stone EM. Best's vitelliform dystrophy. Ophthalmic Paediatr Genet 1990;11:49–59. [PubMed: 2190134]
31. Cross HE, Bard L. Electro-oculography in Best's macular dystrophy. Am J Ophthalmol 1974;77:46–50. [PubMed: 4824173]
32. Pollack K, Kreuz FR, Pillunat LE. Best's disease with normal EOG: case report of familial macular dystrophy. Ophthalmologe 2005;102:891–894. [PubMed: 15657694]
33. Renner AB, Tillack H, Kraus H, et al. Late onset is common in Best macular dystrophy associated with *VMD2* gene mutations. Ophthalmology 2005;112:586–592. [PubMed: 15808248]
34. Marmorstein AD, Stanton JB, Yocom J, et al. A model of best vitelliform macular dystrophy in rats. Invest Ophthalmol Vis Sci 2004;45:3733–3739. [PubMed: 15452084]
35. Marmorstein LY, Wu J, McLaughlin P, et al. The light peak of the electroretinogram is dependent on voltage-gated calcium channels and antagonized by bestrophin (Best-1). J Gen Physiol 2006;127:577–589. [PubMed: 16636205]
36. Bakall B, Marmorstein LY, Hoppe G, et al. Expression and localization of bestrophin during normal mouse development. Invest Ophthalmol Vis Sci 2003;44:3622–3628. [PubMed: 12882816]
37. Marmorstein AD, Kinnick TR. Focus on molecules: bestrophin (Best-1). Exp Eye Res. In press
38. Marquardt A, Stohr H, Passmore LA, et al. Mutations in a novel gene, *VMD2*, encoding a protein of unknown properties cause juvenile-onset vitelliform macular dystrophy (Best's disease). Hum Mol Genet 1998;7:1517–1525. [PubMed: 9700209]

39. Kramer F, White K, Pauleikhoff D, et al. Mutations in the *VMD2* gene are associated with juvenile-onset vitelliform macular dystrophy (Best disease) and adult vitelliform macular dystrophy but not age-related macular degeneration. Eur J Hum Genet 2000;8:286–292. [PubMed: 10854112]

40. Maquat LE. When cells stop making sense: effects of nonsense codons on RNA metabolism in vertebrate cells. RNA 1995;1:453–465. [PubMed: 7489507]

41. Ciulla TA, Frederick AR Jr. Acute progressive multifocal Best's disease in a 61-year-old man. Am J Ophthalmol 1997;123:129–131. [PubMed: 9186112]

42. Hebel R. Development and structure of the retina and the tape-tum lucidum in the dog. Ergeb Anat Entwicklungsgesch 1971;45:3–92. [PubMed: 5146431]

43. Sutter NB, Eberle MA, Parker HG, et al. Extensive and breed-specific linkage disequilibrium in *Canis familiaris*. Genome Res 2004;14:2388–2396. [PubMed: 15545498]

44. Hoppe, G.; Marmorstein, LY.; Marmorstein, AD. Localization and functional analysis of bestrophin. In: Anderson, RE.; LaVail, MM.; Hollyfield, JG., editors. New Insights into Retinal Degenerative Diseases. Kluwer Academic/Plenum Publishers; New York: 2001.

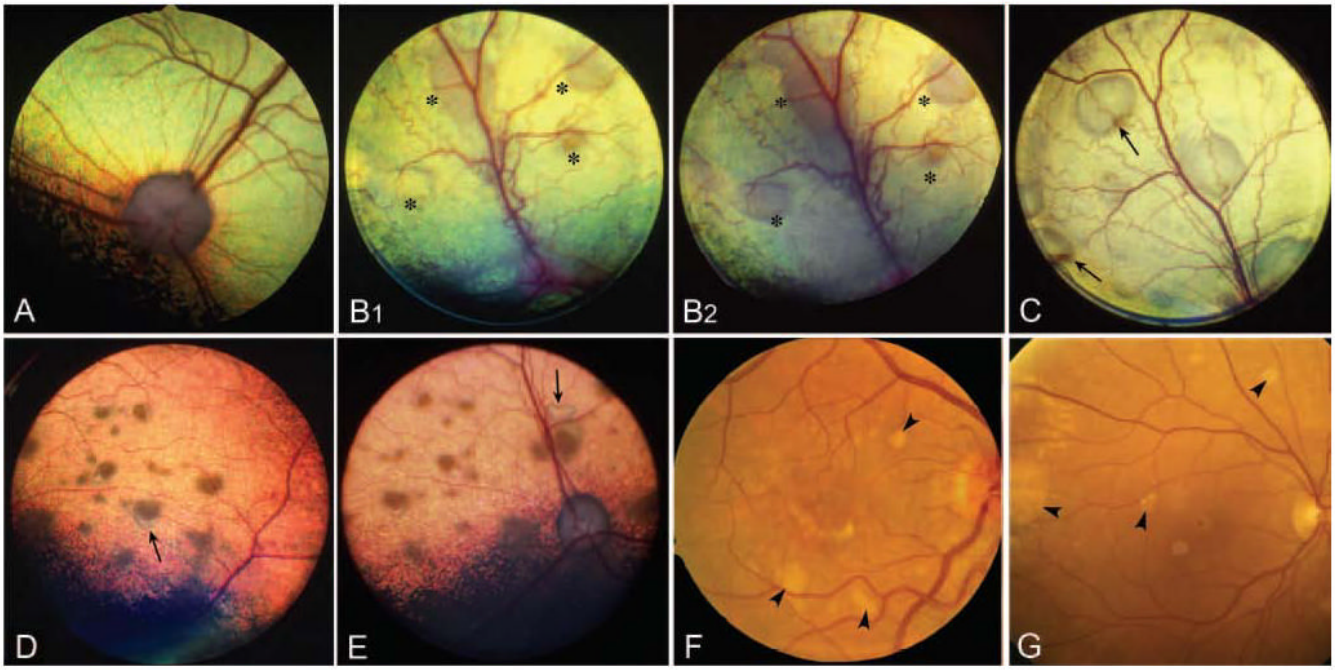

Figure 1.

Fundus photographs illustrating the salient retinal findings of *cmr1* and *cmr2* and multifocal Best disease. (**A**) Healthy control showing that the fundus is divided into the superior tapetal and the inferior nontapetal regions. In the tapetal region, the retinal pigment epithelium in nonpigmented, and overlies the brightly reflective tapetal layer of the choroid. (**B**) Great Pyrenees with *cmr1* at 5 (**B_1**) and 8 (**B_2**) months of age. Retinal lesions (*) are more distinct at 8 months of age. (**C**) Eighteen-month-old Coton de Tulear with *cmr2*. The fluid in the subretinal elevations is clear, though two lesions (*arrows*) show accumulation of a *tan-pink* material in the dependent portion of the blebs. (**D–E**) Fifteen-month-old Coton de Tulear with *cmr2*. Multifocal retinal lesions have *tan-pink brown* subretinal material. Adjacent to several lesions (*arrows*) the subretinal fluid is serous. (**F–G**) Multifocal Best disease in humans shown in 30° and 60° fundus photographs of patients with heterozygous A243T (**F**, 30°) and Y227N (**G**, 60°) mutations. Multifocal lesions (*arrowheads*) are present in both eyes.

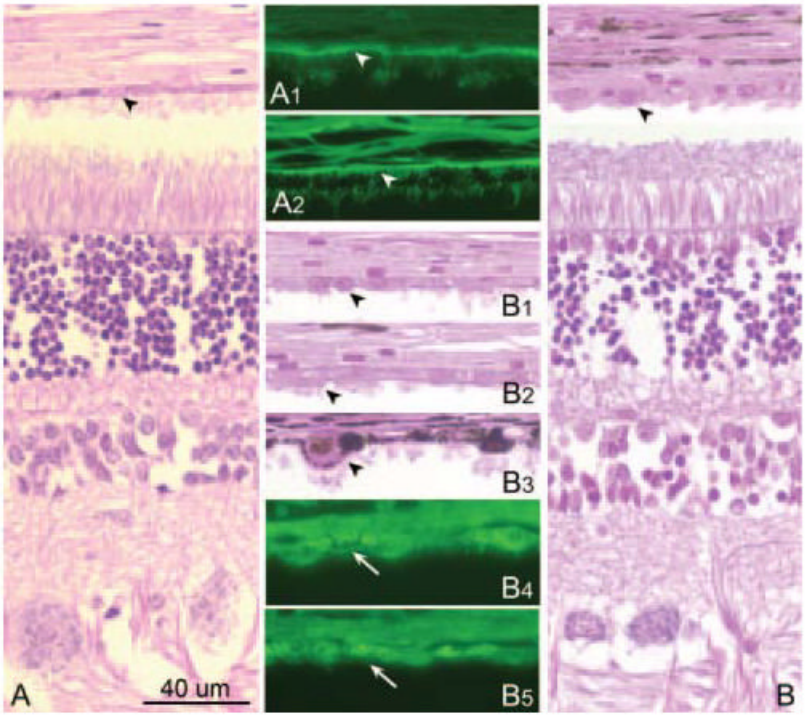

Figure 2.

Samples of normal (**A**, 1 year) and affected (*VMD2* stop mutation; **B**, 4 years) Great Pyrenees dogs. The normal RPE is not hypertrophied (**A**) and shows uniform autofluorescence in the basal zone (*arrowheads*,$\mathbf{A_1}$,$\mathbf{A_2}$). The affected RPE is hypertrophied (*arrowheads*; **B**, $\mathbf{B_1}$–$\mathbf{B_3}$), and bright autofluorescent granules occupy the cytoplasm (*white arrows*; $\mathbf{B_4}$, $\mathbf{B_5}$).

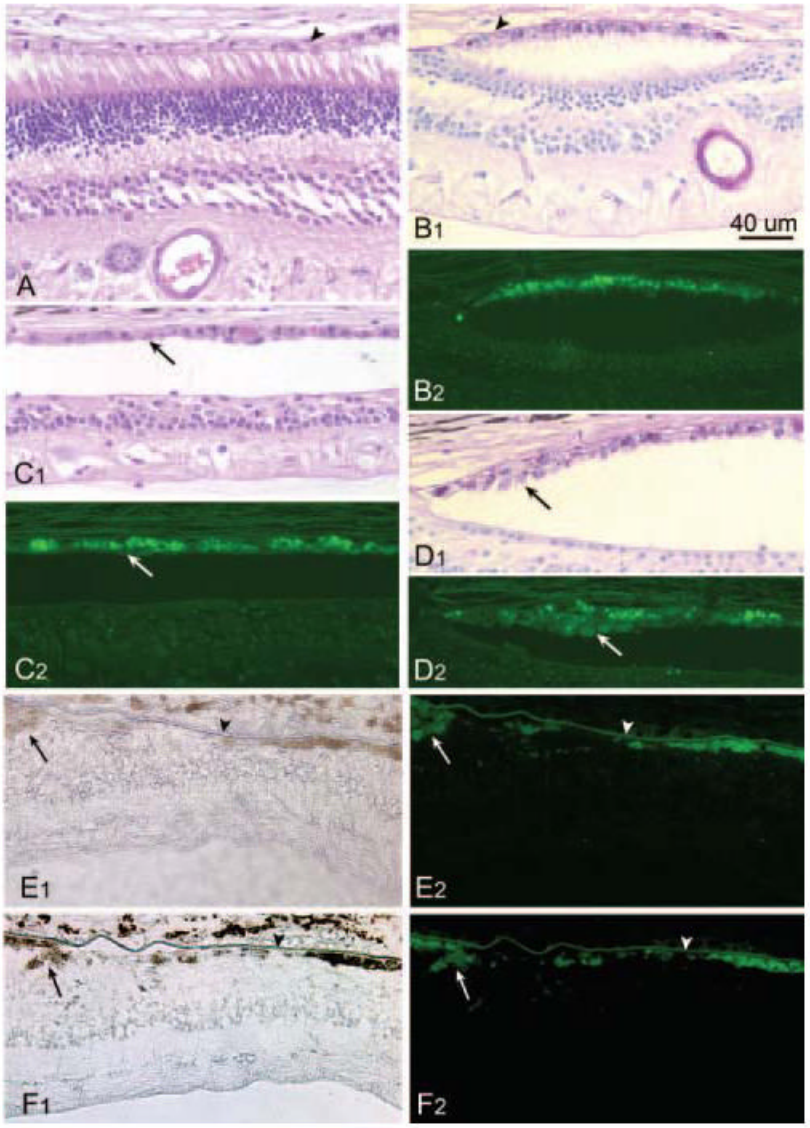

Figure 3.

Retinal pathology in *cmr1* and Best disease. (**A**–**D**) Photomicrographs from archival sample of 10-year-old affected (*VMD2*stop mutation) Great Pyrenees dog. The retina in localized areas of the posterior pole is normal (**A**), though most areas show outer retinal atrophy with RPE cells hypertrophy (**B**–**D**). The RPE cells have granular to *tan-brown* cytoplasmic inclusions (**B_1, C_1, D_1**) that are PAS+ (**B_1, D_1**) and autofluorescent (**B_2, C_2, D_2**). Proliferation of RPE leads to the formation of cell nests (**D_1, D_2**). (**E**–**F**) Photomicrographs of the juxtafoveal region of the retina from an 86-year-old patient with a T6R mutation in *VMD2*. Clusters of pigmented cells are present (*arrows*), and extensive intracytoplasmic lipofuscin accumulation results in bright granular autofluorescence. Areas of photoreceptor loss are associated with regions of RPE dropout, but BM is intact (*arrowheads*).

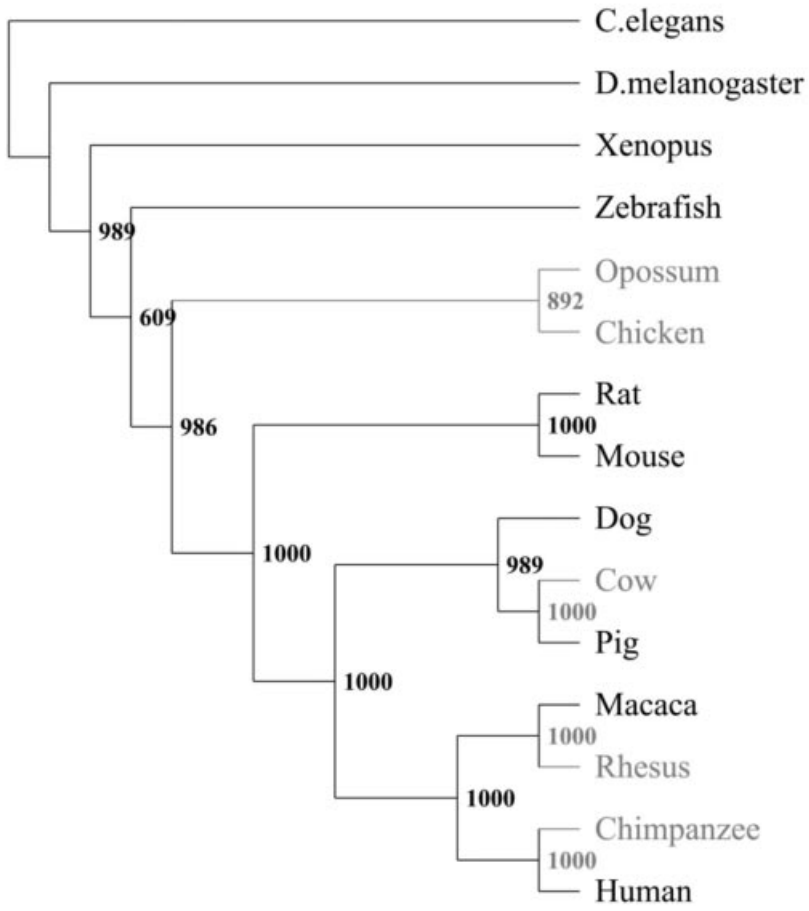

Figure 4.
Sequence divergence of *VMD2* in 14 different species. The neighbor-joining tree was derived from a bootstrapped (n = 1000) F84 model using experimental data (*black*) and predicted gene sequences, where applicable (*gray*).

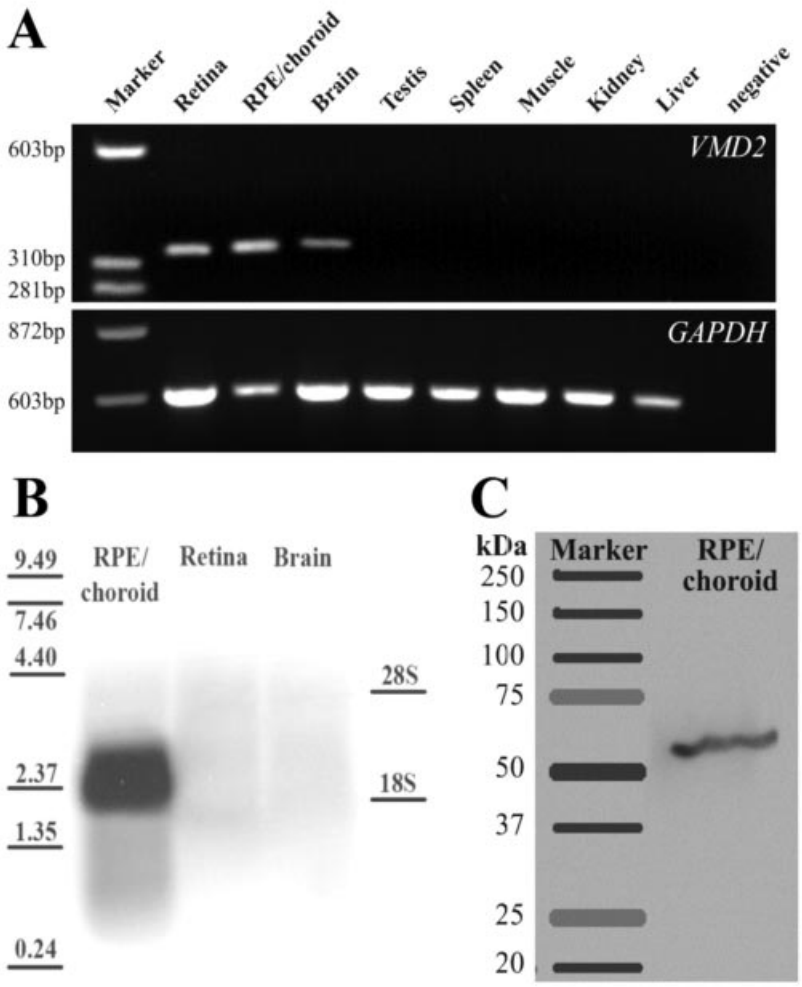

Figure 5.

Expression of *VMD2*-specific transcripts. (**A**) *VMD2* expression in eight canine tissues by RT-PCR. PCR products in RPE/choroid, retina and brain contained the cDNA fragment of expected size (329 bp); *GAPDH* control. (**B**) Northern blot of *VMD2* expression detected the approximately 2.1-kb transcript only in RPE/choroid. (**C**) Western blot analysis with monoclonal E6–6 antibody showed a single band of approximately 60 kDa in the normal canine RPE/choroid sample.

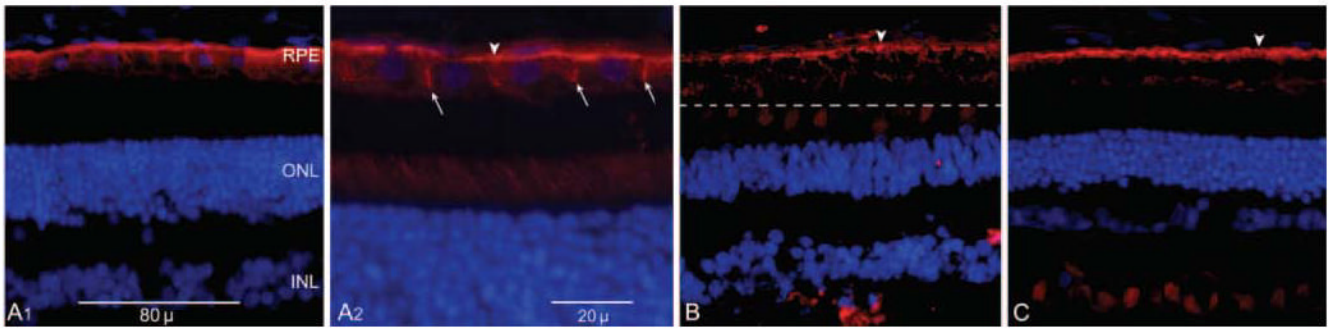

Figure 6.

Immunohistochemistry showing the localization of bestrophin (*red*) in the RPE of *C. familiaris* (**A$_1$**–**A$_2$**), *M. fascicularis* (**B**), and *F. catus* (**C**). The protein is highly expressed in the basolateral membranes of the retinal pigment epithelium (RPE) but not in other retinal layers or the choroid. Nuclei are stained *blue* with DAPI. *Dashed line* (**B**): the apposition of the artifactually separated retina to the RPE. ONL, outer nuclear layer; INL, inner nuclear layer. Scale bars: 80 µm (**A$_1$**, **B**, **C**); 20 µm (**A$_2$**).

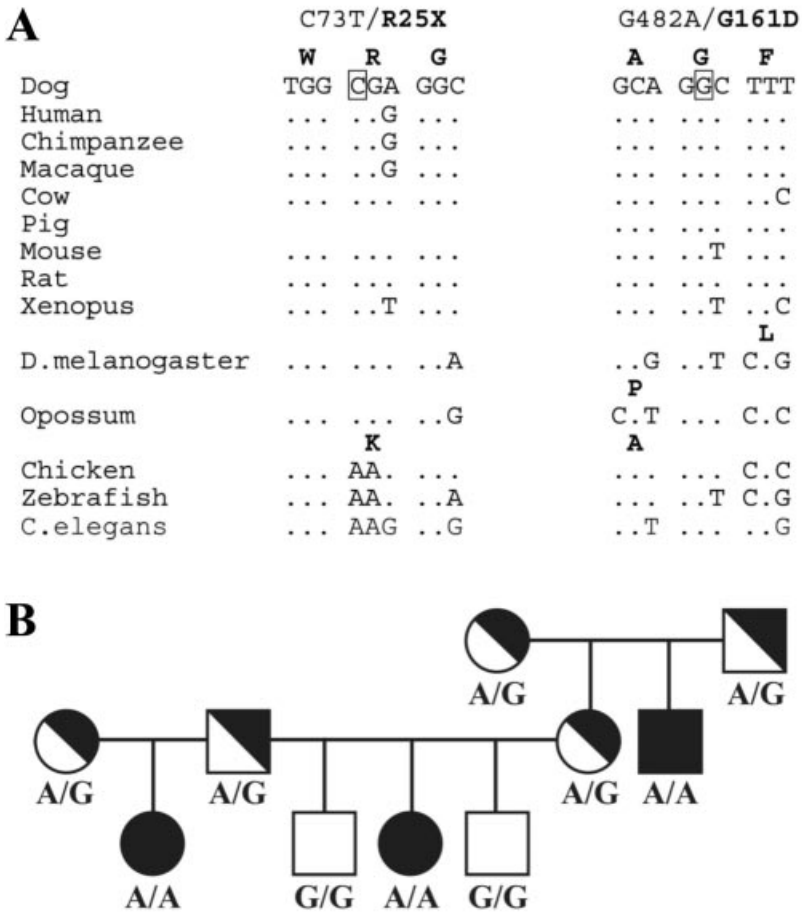

Figure 7.

Identification and cosegregation of the canine *VMD2* gene mutations. (**A**) Conservation of the sequences surrounding the mutation $C_{73}T$ (R_{25}Stop) of *cmr1* and the $G_{482}A$ ($G_{161}D$) change of *cmr2* in 14 *VMD2* orthologs. (**B**) Part of the Coton de Tulear pedigree segregating *cmr2* with recessive inheritance of mutant allele (G, normal allele; A, mutant allele). Clinically evident fundus abnormalities are noticeable in homozygous mutant (A/A) dogs but not in heterozygotes (A/G).